Radiology

Impact of Data-driven Respiratory Gating in Clinical PET[1]

Florian Büther, PhD
Thomas Vehren, MD
Klaus P. Schäfers, PhD
Michael Schäfers, MD

Purpose: To study the feasibility and impact of respiratory gating in positron emission tomographic (PET) imaging in a clinical trial comparing conventional hardware-based gating with a data-driven approach and to describe the distribution of determined parameters.

Materials and Methods: This prospective study was approved by the ethics committee of the University Hospital of Münster (AZ 2014–217-f-N). Seventy-four patients suspected of having abdominal or thoracic fluorine 18 fluorodeoxyglucose (FDG)-positive lesions underwent clinical whole-body FDG PET/computed tomographic (CT) examinations. Respiratory gating was performed by using a pressure-sensitive belt system (belt gating [BG]) and an automatic data-driven approach (data-driven gating [DDG]). PET images were analyzed for lesion uptake, metabolic volumes, respiratory shifts of lesions, and diagnostic image quality.

Results: Forty-eight patients had at least one lesion in the field of view, resulting in a total of 164 lesions analyzed (range of number of lesions per patient, one to 13). Both gating methods revealed respiratory shifts of lesions (4.4 mm ± 3.1 for BG vs 4.8 mm ± 3.6 for DDG, $P = .76$). Increase in uptake of the lesions compared with nongated values did not differ significantly between both methods (maximum standardized uptake value [SUV_{max}], +7% ± 13 for BG vs +8% ± 16 for DDG, $P = .76$). Similarly, gating significantly decreased metabolic lesion volumes with both methods (−6% ± 26 for BG vs −7% ± 21 for DDG, $P = .44$) compared with nongated reconstructions. Blinded reading revealed significant improvements in diagnostic image quality when using gating, without significant differences between the methods (DDG was judged to be inferior to BG in 22 cases, equal in 12 cases, and superior in 15 cases; $P = .32$).

Conclusion: Respiratory gating increases diagnostic image quality and uptake values and decreases metabolic volumes compared with nongated acquisitions. Data-driven approaches are clinically applicable alternatives to belt-based methods and might help establishing routine respiratory gating in clinical PET/CT.

Online supplemental material is available for this article.

[1] From the Department of Nuclear Medicine, University Hospital of Münster, Albert-Schweitzer-Campus 1, 48149 Münster, Germany (F.B., T.V., M.S.); European Institute for Molecular Imaging, University of Münster, Münster, Germany (F.B., K.P.S., M.S.); and DFG EXC 1003 Cluster of Excellence "Cells in Motion," University of Münster, Münster, Germany (K.P.S., M.S.). Received September 18, 2015; revision requested November 4; revision received December 10; accepted January 20, 2016; final version accepted January 21. **Address correspondence to** F.B. (e-mail: *butherf@uni-muenster.de*).

Study supported by Deutsche Forschungsgemeinschaft (SFB 656, projects B02, B03, C06).

Although sensitivities of positron emission tomography (PET) systems have continuously improved in the past few years, it is still necessary to scan a single bed position for a few minutes to acquire sufficient PET coincidence data. Therefore, respiratory motion of organs is highly relevant in clinical PET scanning, as it leads to blurring in PET images, a loss in effective resolution, and inaccuracies in the quantification of tracer uptake (1,2). This is especially the case for lesions located in organs close to the diaphragm, as the magnitude of respiratory shifts is largest there; however, even the apex of the lungs or the lower abdomen is known to be involved in respiratory motion. Correcting for respiratory motion is a challenge because it locally differs in terms of amplitude and frequency and between individual patients.

The most widely investigated concept to overcome motion-induced image degradation is gating of PET data (3,4). Here, the measured PET data are sorted according to a respiratory signal into image subsets (respiratory phases) containing virtually no respiratory motion. Several hardware-based systems to record respiratory signals have been described in the literature (3–6). Clinically, two systems are established: the real-time position management system (Varian Medical Systems, Palo Alto, Calif), which relies on an infrared camera monitoring the anteroposterior motion of a marker placed on the patient's abdomen (7), and the respiratory gating system AZ-733 V (Anzai Medical, Tokyo, Japan), where a pressure sensor installed in a belt and fixed around the patient's belly measures respiration-induced pressure changes (8). Nevertheless, despite its wide availability, gating has not become a standard procedure in clinical PET, because it is often considered complicated and time consuming.

Recently, several gating methods that are driven by the measured PET raw data have been developed (9–13). These approaches result in respiratory signals that are potentially as accurate as those from conventional hardware-based gating methods while not requiring any additional installation time or effort. Data-driven methods assess organ motion rather than body surface motion (as in external measurements) and might therefore lead to different gating results (14). However, to our knowledge, the clinical value of hardware-driven versus data-driven gating [DDG] methods has not yet been systematically studied.

We studied the feasibility and impact of respiratory gating on PET imaging in a clinical trial in which we compared conventional hardware-based gating with a data-driven approach and described the distribution of determined parameters.

Advance in Knowledge

- Data-driven gating and conventional hardware-based gating seem to perform similarly on average in terms of increased lesion uptake, motion resolution, and diagnostic quality and decreased metabolic volumes (range of *P* values, .17–.76); however, as the observed effect sizes were small, the power of this study was found to be too small to potentially reveal significant differences.

Materials and Methods

Software to extract the belt signal from the acquired data were provided by Siemens Healthcare (Erlangen, Germany). All authors had control of the data and of the information submitted for publication.

Patient Data and Preparation

The study protocol was approved by the ethics committee of the University Hospital of Münster. Patients were enrolled consecutively from March to August 2014.

Implication for Patient Care

- Automatic data-driven respiratory gating in PET removes the necessity of installing additional hardware in conventional hardware-based gating.

Patients who were referred for a whole-body fluorine 18 fluorodeoxyglucose (FDG) PET/computed tomographic (CT) examination were included in this prospective study if at least one PET-positive lesion in the thorax or upper abdomen was suspected on the basis of prior CT or PET/CT studies. PET data from 74 patients (30 female, 44 male; age: 55.4 years ± 15.1, body mass: 78.2 kg ± 16.7) were included. Clinical indications for PET/CT examinations were bronchial carcinomas in 19 patients (25.7%), metastases in the lung or mediastinum in 17 patients (23.0%), lymphomas in 24 patients (32.4%), other solid tumors in the thorax (esophagus, thymus, heart) in seven patients (9.5%), and other solid tumors in the upper abdomen (liver, gallbladder, pancreas, adrenal glands) in seven patients (9.5%).

Patients fasted overnight before the examination. An intravenous dose of 4 MBq FDG per kilogram of body weight was injected 60 minutes before the PET scan (Biograph mCT; Siemens Healthcare [15]).

Data Acquisition

For PET/CT data acquisitions, patients were placed in the supine position with

Published online before print
10.1148/radiol.2016152067 **Content code:** NM

Radiology 2016; 281:229–238

Abbreviations:
BG = belt gating
DDG = data-driven gating
FDG = fluorine 18 fluorodeoxyglucose
NAC = non–attenuation corrected
SUV = standardized uptake value
SUV_{max} = maximum SUV
SUV_{mean} = mean SUV

Author contributions:
Guarantors of integrity of entire study, F.B., M.S.; study concepts/study design or data acquisition or data analysis/interpretation, all authors; manuscript drafting or manuscript revision for important intellectual content, all authors; approval of final version of submitted manuscript, all authors; agrees to ensure any questions related to the work are appropriately resolved, all authors; literature research, F.B., T.V., K.P.S.; clinical studies, T.V., K.P.S., M.S.; statistical analysis, all authors; and manuscript editing, all authors

Conflicts of interest are listed at the end of this article.

See also Kesner et al in this issue.

arms above the head. The respiratory gating system AZ-733 V was used to measure respiratory signals during the examination (belt gating [BG]). Application of the belt was performed by a trained physician.

Whole-body CT data (tube voltage, 100 kV; effective current, 20–30 mAs; estimated dose, 1–2 mGy; pitch, 1.25; section thickness, 3.0 mm; rotation time, 0.5 second; scan time, 10–20 seconds) were acquired in end expiration and were used for PET attenuation correction. Whole-body PET data were then acquired with four to six bed positions with 2 minutes each, unless the positions contained the suspected lesions. These were scanned for 6 minutes each, reconstructed separately without and with gating, and further analyzed. To retain any temporal information used during gating, PET data were acquired in list mode rather than in standard sinogram mode to enable retrospective respiratory gating, thus saving every single measured coincidence event in a time-ordered file instead of a histogram.

Respiratory Gating and Data Reconstruction

An automatic DDG approach based on the geometric sensitivity method (10,11), the Kesner algorithm (12), and the segmented center-of-mass approach (13) were used for further gating. The decision as to which algorithm's signal was used for DDG was based on the calculation of the respiratory weight H (as defined in [16]) of the sensitivity and the center-of-mass signals, respectively. If the maximum H value was larger than 2.5, the corresponding signal was considered to be accurate enough and the respective method was subsequently used; otherwise, the signal from the Kesner method was used. Further information is given in Appendix E1 (online). Approximate calculation times of the DDG signals were additionally assessed.

In addition to standard nongated reconstruction using 100% of the measured data (NG100), we created nongated list-mode data sets that contained a randomly chosen 35% of the original emission events to differentiate between statistic- and gating-derived differences (NG35).

In the case of BG and DDG, three amplitude-based gates were computed: *(a)* the "optimal gate" (17,18), representing 35% of the data recorded during the least motion-contaminated respiratory phase (HD-Chest option of the scanner); *(b)* the maximum expiratory gate, representing 35% of data with the lowest signal amplitude; and *(c)* the maximum inspiratory gate, representing 35% of data with the highest signal amplitude.

In the case of two adjacent bed positions, the latter two required that both DDG signals have the same orientation in terms of expiration and inspiration. This was solved in a similar manner as described earlier (19) and relies on the Kesner gating method, where every sinogram cluster is assigned a weighting factor (−1, 0, or +1). Owing to the overlap of adjacent bed positions, it is possible to compare these weighting factors for segment 0 sinogram clusters for identical real world z coordinates. A positive correlation coefficient demonstrates that both signals have the same orientation, while a negative one means that one signal has to be multiplied by −1 to result in the same orientation.

An iterative three-dimensional time-of-flight ordered subsets expectation maximization algorithm with two iterations and 21 subsets, scatter correction, and a 2-mm postreconstruction Gaussian filter was used to reconstruct the different data sets, resulting in images of 200 × 200 × 174 (two bed positions) or 200 × 200 × 112 (one bed position) voxels of 4 × 4 × 2 mm.

Data Analysis

Images were first analyzed for FDG-positive lesions by a nuclear medicine physician (T.V., with 5 years of experience in PET image diagnosis). Apparent respiratory shifts between maximum expiration and maximum inspiration for these lesions were measured as described previously (13,16) (see Appendix E2 [online] for further information). Additionally, maximum standardized uptake value (SUV) (SUV_{max}), mean SUV (SUV_{mean}), and lesion volume (based on a 40% SUV_{max} threshold) were determined by using Siemens SyngoVia. SUV_{max} values were also determined from the non–attenuation-corrected (NAC) images. Finally, the overall diagnostic quality of the nongated and the HD-Chest–gated PET image data sets were assessed by four readers: two nuclear medicine physicians with 6 (A.V.) and 20 (M.S.) years of experience in PET image diagnosis and two medical physicists with 10 years of experience in motion-related PET image artifacts (K.P.S., F.B.). For this purpose, coronal sections of gated and nongated image data sets through each lesion were prepared by author T.V. Each reader was independently asked to rank the relative quality of the four randomly combined images (NG100, NG35, BG, and DDG, with the readers being blinded to the methods) in terms of lesion delineation and motion blurring for each lesion from worst to best (allowing equal quality). This allowed us to extract relative scores for every pairwise comparison of methods for every lesion and reader (eg, −1 if BG was inferior to DDG, 0 if BG and DDG performed equally, +1 if BG was superior). For cases with multiple lesions, the mean relative quality score per reader and comparison was determined and set to −1 for negative values, +1 for positive values, and 0 otherwise. Similarly, the mean relative score per scan and comparison was determined by averaging all four readers' ratings.

Apparent outliers in quantitative parameters, indicating problems with a gating method, were further assessed for irregularities in gating signals by F.B.

Statistical analysis was performed by using all lesions found, and, separately, by using one fixed reference lesion per scan. The latter was determined by computing a random number from a discrete uniform distribution over the interval 1,…,n (n: number of lesions per scan) with MATLAB (version 2013b; MathWorks, Natick, Mass) and then choosing the lesion with the respective number from the list of identified lesions for that scan.

Furthermore, we analyzed respiratory shifts for the lesions closest to the diaphragm (if present), as respiratory motion is assumed to be greatest in this region. Testing for significant differences in values was done by performing paired two-tailed Wilcoxon signed-rank tests (for respiratory shifts, SUV, and volumes) and sign tests (for visual quality) by using the statistical toolbox in MATLAB. A Holm-Bonferroni correction for pairwise comparisons was applied to compensate for the growth of the family-wise error rate when performing multiple tests (20). The family-wise error rate was set to .05, and the Holm-Bonferroni correction was performed for 31 comparisons in both the reference lesion group and the total lesion group.

Prior to the study, no data on expected effect sizes and distributions with regard to the patient cohort of this study and to the specific gating method were available; therefore, no a priori sample size calculation was performed. Instead, a post-hoc power calculation based on the determined effect sizes (Cohen *d*) and distributions in the reference lesion group was performed by using the free tool G*Power (21).

Results

Of the overall 74 PET/CT studies, 43 were acquired in a single bed position and 31 were acquired in two bed positions for gating. For DDG analysis, a sensitivity-based signal was used for 24 list-mode scans, the signal based on the Kesner method was used for 32 scans, and the signal based on the segmented center-of-mass approach was used in 49 scans. Computation of the final DDG signal took less than 5 minutes per list-mode scan.

PET-positive lesions were found in 48 of the 74 patients in a total of 64 list-mode scans. In total, 164 lesions were identified. Table 1 summarizes these lesions.

Quantitative comparison of respiratory shifts, uptake values, and lesion volumes for these 164 lesions are shown in Table 2. The mean respiratory shift as measured in the NAC gated images was 4.6 mm ± 3.2 for BG versus 4.9 mm ± 3.6 for DDG. SUV_{max} was 9.7 ± 7.2 for NG100 and 10.3 ± 7.6 for NG35 (Fig 1). Gating significantly increased SUV_{max}, with 10.7 ± 7.6 for BG and 10.7 ± 7.8 for DDG, corresponding to a mean increase against NG35 of +7% ± 16 for BG and +6% ± 15 for DDG. SUV_{mean} was 5.9 ± 4.4 for NG100 and 6.0 ± 4.6 for NG35 (Fig 1) and increased to 6.3 ± 4.6 for BG and 6.3 ± 4.7 for DDG. Lesion volumes were 18.8 mL ± 52.8 for NG100 and 17.2 mL ± 48.4 for NG35 (Fig 1) and decreased to 15.5 mL ± 44.1 for BG and 16.0 mL ± 45.3 for DDG, corresponding to a mean decrease against NG35 of 7% ± 25 for BG and 5% ± 21 for DDG. SUV_{max} values in the NAC images were 2446 kBq/mL ± 1732 for NG100, 2537 kBq/mL ± 1770 for NG35, 2684 kBq/mL ± 1795 for BG, and 2691 kBq/mL

Table 1

Characteristics of All 164 Lesions Analyzed in This Study

Location	No. of Lesions/No. of Patients	Metabolic Volume (mL)	SUV_{max}	Respiratory Shift (mm)
Upper lungs	19/11	8.1 ± 24.3	10.8 ± 9.3	3.8 ± 2.4
Upper mediastinum	49/25	5.5 ± 7.8	8.0 ± 5.1	3.6 ± 1.7
Lower mediastinum	21/15	26.7 ± 55.3	11.1 ± 6.7	4.5 ± 1.8
Lower lungs	31/13	14.0 ± 45.2	10.1 ± 7.9	8.4 ± 4.8
Abdomen (infradiaphragmatic)	39/15	42.5 ± 86.1	11.0 ± 8.0	6.1 ± 3.7
Other locations	5/4 (One in breast, one in sternum, three in ribs)	2.7 ± 1.6	4.4 ± 1.4	2.0 ± 1.4
Total	164/48	18.8 ± 52.8	9.7 ± 7.1	5.2 ± 3.6

Note.—Unless otherwise specified, data are means ± standard deviations. Volumes and SUV_{max} were determined from the NG100 images, and respiratory shift of a single lesion was defined as the maximum shift value determined from either the BG or the DDG images.

Table 2

Values for Respiratory Shifts, Uptake, and Lesion Volumes in the NG100, NG35, BG, and DDG Images of All 164 Lesions

Parameter	NG100	NG35	BG	DDG
Mean respiratory shift (mm)			4.6 ± 3.2	4.9 ± 3.6
P value vs BG35				.15
Mean NAC SUV_{max}	2446 ± 1732	2537 ± 1770	2684 ± 1795	2691 ± 1855
P value vs NG100		<.0001	<.0001	<.0001
P value vs NG35			<.0001	<.0001
P value vs BG35				.28
Mean SUV_{max}	9.7 ± 7.2	10.3 ± 7.6	10.7 ± 7.6	10.7 ± 7.8
P value vs NG100		<.0001	<.0001	<.0001
P value vs NG35			<.0001	<.0001
P value vs BG35				.22
Mean SUV_{mean}	5.9 ± 4.4	6.0 ± 4.6	6.3 ± 4.6	6.3 ± 4.7
P value vs NG100		<.0001	<.0001	<.0001
P value vs NG35			<.0001	<.0001
P value vs BG35				.15
Mean volume (mL)	18.8 ± 52.8	17.2 ± 48.4	15.5 ± 44.1	16.0 ± 45.3
P value vs NG100		<.0001	<.0001	<.0001
P value vs NG35			<.0001	<.0001
P value vs BG35				.12

Figure 1

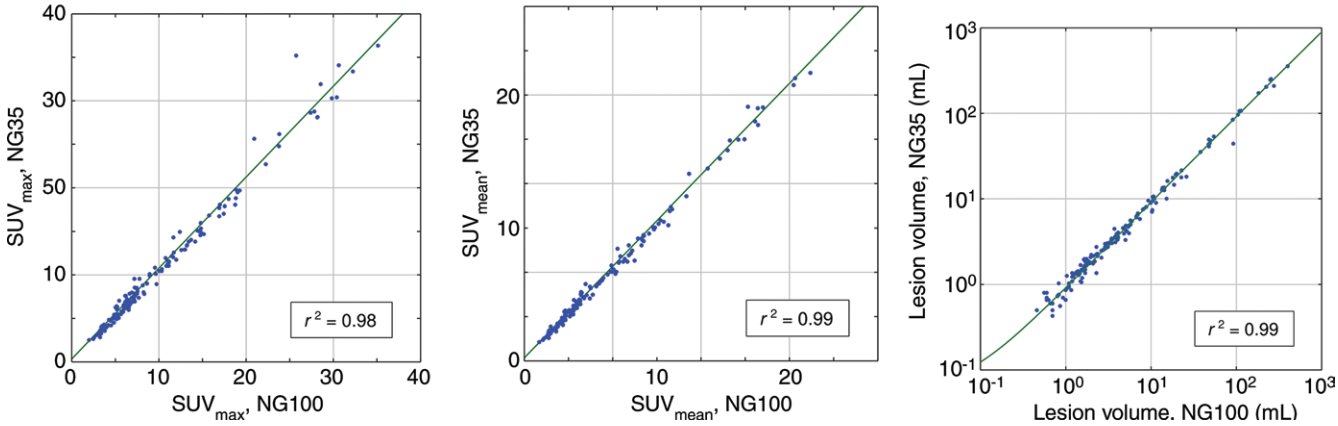

Figure 1: Scatterplots of SUV_{max}, SUV_{mean}, and metabolic volumes of all 164 lesions for NG100 and NG35. Green line: linear fit.

± 1855 for DDG. For all these parameters, only the differences between BG and DDG were found to be statistically nonsignificant; all other comparisons demonstrated significant differences, with $P < .0001$.

Alternatively, when we restricted the analysis to the 48 reference lesions, respiratory shifts (correlation: $r^2 = 0.60$; Fig 2), uptake values (mean SUV_{max} increase against NG35, +7% ± 13 for BG, +8% ± 16 for DDG), and tumor volumes (mean decrease against NG35, 6% ± 26 for BG, 7% ± 21 for DDG) changed little on average (Fig 3), and there was again no significant difference in parameters between BG and DDG, while all other comparisons of determined parameters demonstrated statistically significant differences, with $P < .01$ (Table 3).

Analyzing only the lesions closest to the diaphragm in 34 scans revealed higher mean shifts; on average, DDG values were larger than BG values (5.6 mm ± 3.5 for BG vs 6.7 mm ± 4.7 for DDG, $P = .03$, $r^2 = 0.50$; Fig 2). No significant differences were determined for the other parameters.

Visual assessment of the PET images revealed that no single lesion was exclusively visible in the gated data sets. Moreover, the data-driven approach did not result in additional obvious artifacts or spurious lesions. Pairwise comparison between nongated and gated PET images in coronal views (Fig 4) demonstrated no significant differences in diagnostic image quality between NG100 and NG35 (NG35 was judged inferior to NG100 in 17 cases, equal in 18, and superior in 13; $P = .72$). Furthermore, no significant difference was seen when we compared BG and DDG (DDG was judged inferior to BG in 22 cases, equal in 12, and superior in 15; $P = .32$). All other comparisons (ie, each gated image compared with each nongated image) demonstrated significant differences: BG was judged to be inferior, equal, or superior to NG100 in four, six, and 38 cases, respectively ($P < 0.0001$); DDG was judged to be inferior, equal, or superior to NG100 in eight, six, and 34 cases, respectively ($P < .0001$); BG was judged to be inferior, equal, or superior to NG35 in four, seven, and 37 cases, respectively ($P < .0001$); and DDG was judged to be inferior, equal, or superior to NG35 in four, seven, and 37 cases, respectively ($P = .0003$). Images judged superior demonstrated less motion-related blurring, better lesion delineation, and higher apparent tracer uptake of lesions (Figs 5, 6).

Although on average both gating methods showed a similar performance, there were a few striking cases where DDG outperformed BG. Deeper analysis demonstrated that a

Figure 2

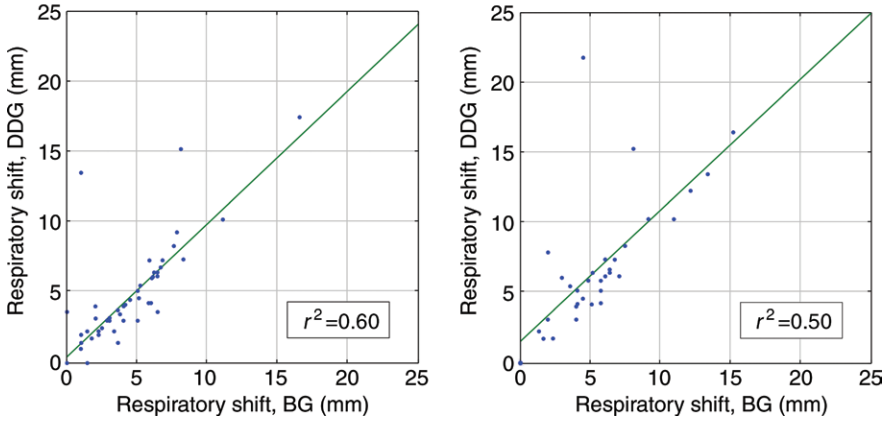

Figure 2: Scatterplots of respiratory shifts of the 48 reference lesions (left) and the 34 lesions closest to the diaphragm (right) for BG and DDG. Green line: linear fit.

Figure 3

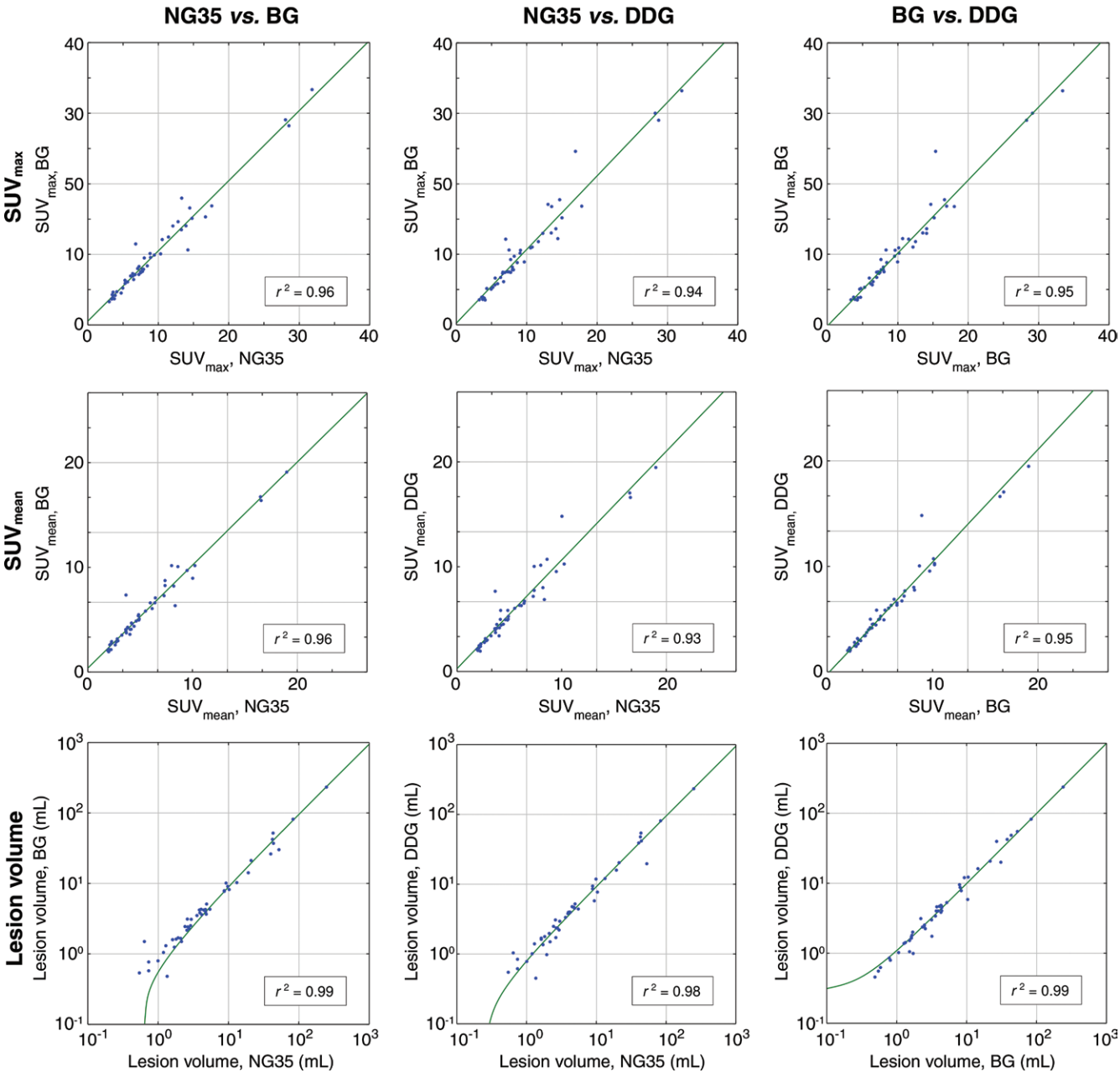

Figure 3: Scatterplots of SUV_{max}, SUV_{mean}, and metabolic volumes of the 48 reference lesions for NG35, BG, and DDG, respectively. Green line: linear fit.

time delay between the recorded belt signal and the data-driven signal was the most likely explanation, as demonstrated in Figure 5. The maximum delay found in those cases amounted to approximately 1 second, which was sufficient to completely suppress the improvement of the gating effort in BG. Manually shifting the original belt curve to the data-driven curve restored most of the respiratory shift resolution and uptake increase compared with DDG.

On the other hand, cases where DDG was substantially inferior to BG were typically characterized by small lesions with relatively low uptake, limited contrast in the emission data, and limited overall respiratory motion (Fig 6).

Power analysis of the reference lesion outcomes demonstrated that effect sizes d for all quantitative parameters in comparisons between

Table 3

Values for Respiratory Shifts, Uptake, Lesion Volumes, and Diagnostic Quality Volumes in the NG100, NG35, BG, and DDG Images of the 48 Reference Lesions

Parameter	NG100	NG35	BG	DDG
Mean respiratory shift (mm)			4.4 ± 3.1	4.8 ± 3.6
P value vs BG				.76
Mean NAC SUV_{max}	2325 ± 1572	2410 ± 1643	2569 ± 1671	2560 ± 1731
P value vs NG100		.0001	<.0001	<.0001
P value vs NG35			.0001	.006
P value vs BG				.17
Mean SUV_{max}	9.3 ± 6.1	9.7 ± 6.4	10.2 ± 6.5	10.5 ± 6.9
P value vs NG100		<.0001	<.0001	<.0001
P value vs NG35			.0008	.0003
P value vs BG				.76
Mean SUV_{mean}	5.5 ± 3.7	5.7 ± 3.8	6.0 ± 3.8	6.1 ± 4.1
P value vs NG100		.0002	<.0001	<.0001
P value vs NG35			.0008	.0003
P value vs BG				0.72
Mean volume (mL)	17.6 ± 40.6	15.8 ± 38.9	14.6 ± 37.4	14.7 ± 37.0
P value vs NG100		<.0001	<.0001	<.0001
P value vs NG35			.003	.003
P value vs BG				.44
Diagnostic quality				
P value vs NG100		.72	<.0001	<.0001
P value vs NG35			<.0001	.0003
P value vs BG				.32

Figure 4

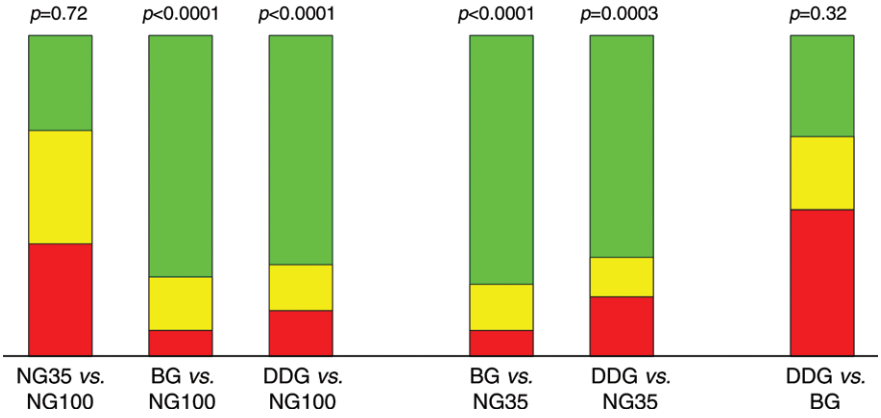

Figure 4: Graph shows pairwise comparison of the diagnostic quality of NG100, NG35, BG, and DDG images in 48 studies. In a comparison of method 1 versus method 2, green areas correspond to the amount of cases where method 1 was judged to be superior to method 2, red areas correspond to cases where method 1 was judged to be inferior to method 2, and yellow areas correspond to cases where no difference in image quality was seen.

BG and DDG were small (0.16 for respiratory shifts, 0.07 for NAC SUV_{max}, 0.17 for SUV_{max}, 0.18 for SUV_{mean}, and 0.05 for volumes). Assuming—as empirically found for all parameters—Laplace distributions for the differences in parameters between DDG and BG, power values were determined as 0.28 for respiratory shifts, 0.09 for NAC SUV_{max}, 0.28 for SUV_{max}, 0.32 for SUV_{mean}, and 0.07 for volumes.

Discussion

This study finds a significant improvement in both diagnostic image quality and the quantification of clinical PET images when respiratory gating is systematically applied in motion-affected regions of the human body.

Respiratory motion of organs—although known for years as a source of image degradation, artifacts, and quantification issues during PET scans—is typically not dealt with in routine clinical scans (14). This is probably caused by several factors. First, correction for respiratory motion requires the installation of hardware (eg, a belt system) for every patient, which even for trained staff members requires additional time. To the same end, respiratory gating requires longer scan times because of the inherent loss of emission data that are discarded for reconstruction. This additional effort and time seem relevant given the typically tight scanning schedule of a PET scanner, especially because the overall benefit of motion correction strategies is not yet clinically exploited. Additionally, although gating leads to better quantification of image-derived measures such as SUV, it may not change diagnoses or staging outcome in a substantial amount of scans because of limited respiratory motion or the additional information gained by CT in hybrid PET/CT systems. Finally, the validity of hardware-based methods to derive respiration information can be questioned, as usually only surrogate motion information (eg, external pressure changes or external marker motion) instead of internal organ or lesion motion information is determined (22,23).

Various software-based DDG approaches have been developed over recent years that may overcome at least some of the obstacles of the hardware-based methods as they might also accurately assess a patient's respiration, and, even better, derive "real" motion information because the analysis is based on emission data from inside the

Figure 5

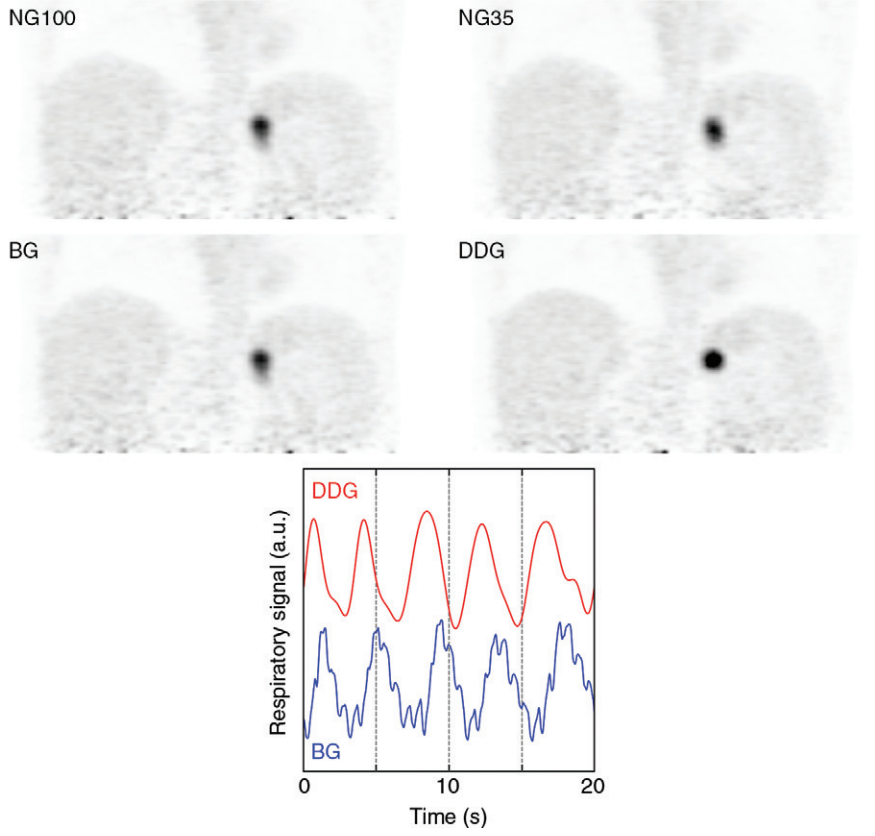

Figure 5: Coronal section of a lesion without gating (top row) and with gating (middle row). SUV_{max} was determined as 15.8, 16.8, 15.3, and 24.5 for NG100, NG35, BG, and DDG, respectively. Analysis of the respiratory curves reveals a delay in the belt signal to the data-driven signal of approximately 1 second (bottom).

body. However, DDG by now has been applied only in proof-of-concept studies in small patient samples; additionally, no larger comparisons against conventional gating methods are available.

In the clinical setting of this study, we found the predicted improvement in diagnostic image quality and quantification through respiratory gating of lesions affected by respiratory motion. On average, no substantial differences in gating efficiency were found between DDG and hardware-driven gating; software-based gating might thus prove to be a substitute for conventional gating in future trials that include more patient scans.

However, we also clearly demonstrate here that hardware-based methods may fail to deliver good motion resolution in some instances. This is reflected by the large variance in outcomes between BG and DDG (especially regarding respiratory shifts, with a comparably low correlation of r^2 = 0.60).

Interestingly, we found in some scans a definite delay between data-driven and belt-based respiration signals. Although we cannot exclude the possibility that this was caused by the technical problems of synchronizing the belt signals with the PET list-mode stream, this observation is much in line with results of previous studies (23–25) and may show fundamental problems with surrogate measurements for respiratory gating, in some cases caused by nonlinear respiratory behavior in some patients (respiratory hysteresis). On the other hand, DDG may underestimate motion if lesions are small and the contrast is low. Taken together, a single gating approach will very likely not give the best results in terms of motion resolution and quantitative accuracy, and a future combination of BG and DDG may be advantageous.

In addition, we show here that decreasing the data statistics used for image reconstruction leads to an increase in SUV and a decrease in lesion volume. This is caused by an elevation in noise levels, making higher image values more likely. This explains why significant changes in SUV and lesion volumes were present when we compared NG100 and NG35, although the latter does not involve any motion correction at all. A part of the increase in SUV when using either gating method is thus caused by higher noise; nevertheless, the differences between gating and NG35 were also significant, demonstrating the predominant effect of motion resolution in those images.

In this study, we chose the amplitude-based HD-Chest gating scheme as a means to reconstruct motion-free images. This was based on previous findings that amplitude-based gating is superior to phase-based gating in terms of motion resolution (4). Additionally, this gating scheme was shown to result in images with acceptable statistical quality in clinical studies (8); however, only 35% of the acquired data are used for image reconstruction with this gating approach.

This emphasizes the inherent disadvantage of all currently clinically available gating algorithms, which is the effective loss of measured PET coincidence data for image reconstruction, leading to higher levels of unwanted image noise. It remains to be seen how DDG will perform in advanced motion-correction schemes integrated in image reconstruction, thus retaining all measured events while still leading to sharp images without motion blur.

Our study had limitations. The number of patients included in this study was too small to allow us to judge whether DDG generally outperforms BG (or vice versa), as evidenced by the small power values achieved. On the basis of the measured effect sizes

Figure 6

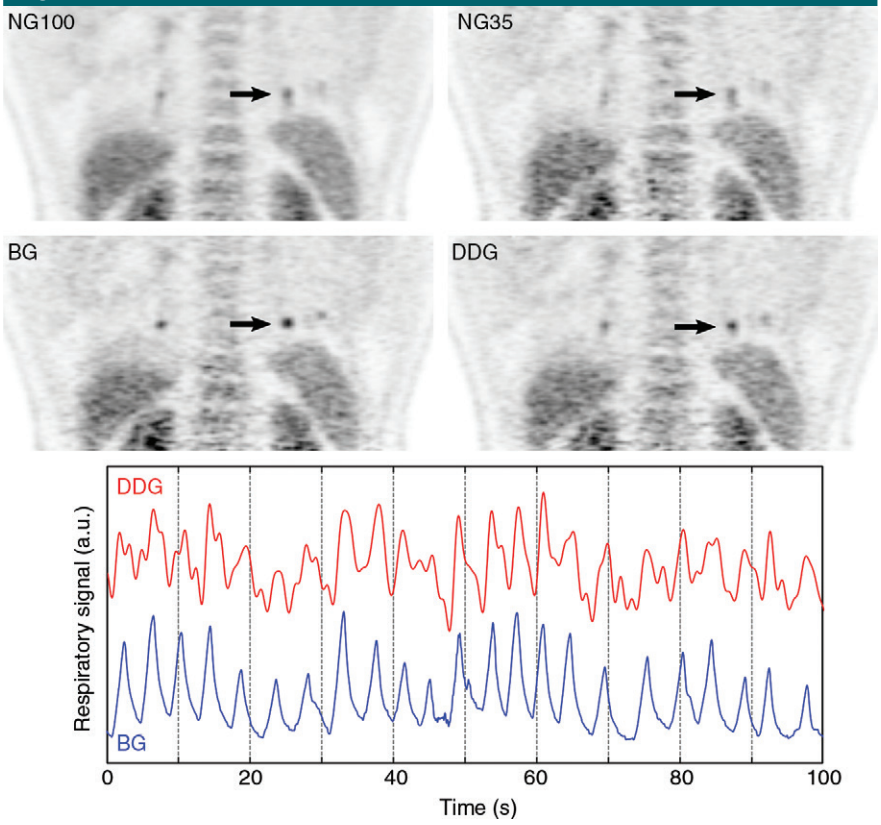

Figure 6: Coronal section of a lesion without gating (top row) and with gating (middle row). SUV_{max} was determined as 3.3, 2.8, 5.5, and 5.0 for NG100, NG35, BG, and DDG, respectively. Analysis of the respiratory curves reveals a comparably poor quality of the data-driven signal (bottom).

in our study, we estimate that at least 150–200 patients with at least one lesion should be scanned in future trials to achieve acceptable power values of 0.8 for SUV_{max}, SUV_{mean}, and respiratory shifts.

In conclusion, respiratory gating in clinical FDG PET/CT studies leads to improved diagnostic image quality and quantification. This effect is independent of the gating method—DDG or BG—applied. Because DDG can easily be added to routine PET scans, it has the potential to promote the clinical application of respiratory gating.

Acknowledgments: The authors thank Alexis Vrachimis, MD, for judging the visual quality of images. Siemens Healthcare (Erlangen, Germany) provided us with software to extract belt signals from acquired data.

Disclosures of Conflicts of Interest: F.B. disclosed no relevant relationships. **T.V.** disclosed no relevant relationships. **K.P.S.** disclosed no relevant relationships. **M.S.** Activities related to the present article: none to disclose. Activities not related to the present article: institution has research grants or grants pending with Siemens Healthcare for molecular imaging. Other relationships: none to disclose.

References

1. Lang N, Dawood M, Büther F, Schober O, Schäfers M, Schäfers K. Organ movement reduction in PET/CT using dual-gated list-mode acquisition. Z Med Phys 2006;16(1):93–100.
2. Liu C, Pierce LA 2nd, Alessio AM, Kinahan PE. The impact of respiratory motion on tumor quantification and delineation in static PET/CT imaging. Phys Med Biol 2009; 54(24):7345–7362.
3. Nehmeh SA, Erdi YE, Ling CC, et al. Effect of respiratory gating on reducing lung motion artifacts in PET imaging of lung cancer. Med Phys 2002;29(3):366–371.
4. Dawood M, Büther F, Lang N, Schober O, Schäfers KP. Respiratory gating in positron emission tomography: a quantitative comparison of different gating schemes. Med Phys 2007;34(7):3067–3076.
5. Klein GJ, Reutter BW, Ho MW, Reed JH, Huesman RH. Real-time system for respiratory-cardiac gating in positron tomography. IEEE Trans Nucl Sci 1998;45(4):2139–2143.
6. Ersepke T, Büther F, Heß M, Schäfers KP. A contactless approach for respiratory gating in PET using continuous-wave radar. Med Phys 2015;42(8):4911–4919.
7. Lupi A, Zaroccolo M, Salgarello M, Malfatti V, Zanco P. The effect of 18F-FDG-PET/CT respiratory gating on detected metabolic activity in lung lesions. Ann Nucl Med 2009;23(2):191–196.
8. Grootjans W, de Geus-Oei LF, Meeuwis AP, et al. Amplitude-based optimal respiratory gating in positron emission tomography in patients with primary lung cancer. Eur Radiol 2014;24(12):3242–3250.
9. Schleyer PJ, O'Doherty MJ, Barrington SF, Marsden PK. Retrospective data-driven respiratory gating for PET/CT. Phys Med Biol 2009;54(7):1935–1950.
10. Büther F, Dawood M, Stegger L, et al. List mode-driven cardiac and respiratory gating in PET. J Nucl Med 2009;50(5):674–681.
11. He J, O'Keefe GJ, Geso M. Motion image compensation based on dynamic data in PET acquisition. J Inf Comput Sci 2010;7(4): 885–891.
12. Kesner AL, Kuntner C. A new fast and fully automated software based algorithm for extracting respiratory signal from raw PET data and its comparison to other methods. Med Phys 2010;37(10):5550–5559.
13. Büther F, Ernst I, Dawood M, et al. Detection of respiratory tumour motion using intrinsic list mode-driven gating in positron emission tomography. Eur J Nucl Med Mol Imaging 2010;37(12):2315–2327.
14. Kesner AL, Schleyer PJ, Büther F, Walter MA, Schäfers KP, Koo PJ. On transcending the impasse of respiratory motion correction applications in routine clinical imaging - a consideration of a fully automated data driven motion control framework. EJNMMI Phys 2014;1(1):8.
15. Jakoby BW, Bercier Y, Conti M, Casey ME, Bendriem B, Townsend DW. Physical and clinical performance of the mCT time-of-flight PET/CT scanner. Phys Med Biol 2011;56(8): 2375–2389.
16. Büther F, Ernst I, Hamill J, et al. External radioactive markers for PET data-driven respiratory gating in positron emission tomography. Eur J Nucl Med Mol Imaging 2013;40(4): 602–614.

17. van Elmpt W, Hamill J, Jones J, De Ruysscher D, Lambin P, Ollers M. Optimal gating compared to 3D and 4D PET reconstruction for characterization of lung tumours. Eur J Nucl Med Mol Imaging 2011;38(5):843–855.

18. Liu C, Alessio A, Pierce L, et al. Quiescent period respiratory gating for PET/CT. Med Phys 2010;37(9):5037–5043.

19. Schleyer PJ, O'Doherty MJ, Marsden PK. Extension of a data-driven gating technique to 3D, whole body PET studies. Phys Med Biol 2011;56(13):3953–3965.

20. Holm S. A simple sequentially rejective multiple test procedure. Scand J Stat 1979;6(2):65–70.

21. Faul F, Erdfelder E, Lang AG, Buchner A. G*Power 3: a flexible statistical power analysis program for the social, behavioral, and biomedical sciences. Behav Res Methods 2007;39(2):175–191.

22. Didierlaurent D, Ribes S, Batatia H, et al. The retrospective binning method improves the consistency of phase binning in respiratory-gated PET/CT. Phys Med Biol 2012;57(23):7829–7841.

23. Dasari PKR, Shazeeb MS, Könik A, et al. Adaptation of the modified Bouc-Wen model to compensate for hysteresis in respiratory motion for the list-mode binning of cardiac SPECT and PET acquisitions: testing using MRI. Med Phys 2014;41(11):112508.

24. Koch N, Liu HH, Starkschall G, et al. Evaluation of internal lung motion for respiratory-gated radiotherapy using MRI: Part I--correlating internal lung motion with skin fiducial motion. Int J Radiat Oncol Biol Phys 2004;60(5):1459–1472.

25. Heß M, Büther F, Gigengack F, Dawood M, Schäfers KP. A dual-Kinect approach to determine torso surface motion for respiratory motion correction in PET. Med Phys 2015;42(5):2276–2286.

Quantitative Assessment of Rectal Cancer Response to Neoadjuvant Combined Chemotherapy and Radiation Therapy

From
Ivana M. Blazic, MD, PhD,* Gordana B. Lilic, MD,† and Milan M. Gajic, PhD‡
Department of Radiology, Memorial Sloan-Kettering Cancer Center, 1275 York Ave, New York, NY 10065-6007*
e-mail: *ivanablazic@yahoo.com*
Center for Radiology and MRI, Clinical Center of Serbia, Belgrade, Serbia†
Institute for Medical Statistics and Informatics, Belgrade, Serbia‡

Editor

Concerning our recent study in *Radiology* (1), published online ahead of print on June 2, we believe that there are a number of issues that need to be clarified.

It has come to our attention that we inadvertently neglected to state that five subjects included in this study (1) were also included in a study we previously published in the *Croatian Medical Journal* (2). The latter study assessed the accuracy of magnetic resonance diffusion-weighted imaging in evaluating the degree of rectal cancer response after therapy (assessment of tumor downstaging), while the former study evaluated the accuracy of different apparent diffusion coefficient measurement methods in predicting complete tumor response to neoadjuvant treatment.

Also, we would like to clarify that the top left and top middle subfigures in Figure 2 and the bottom left subfigure in Figure 3 published in the article in the *Croatian Medical Journal* (2) have been reproduced in the article published in the *Radiology* (1) as the top left and bottom left subfigures in Figure 1 and the top left subfigure in Figure 2. The study in the *Croatian Medical Journal* was published under a Creative Common License that gives authors the right to reproduce components of their article, including figures.

The article has been updated to correct these oversights, and an erratum has been issued for the earlier ahead of print version. The final correct version of the article appears in this issue of the journal.

Disclosures of Conflicts of Interest: I.M.B. disclosed no relevant relationships. **G.B.L.** disclosed no relevant relationships. **M.M.G.** disclosed no relevant relationships.

References

1. Blazic IM, Lilic GB, Gajic MM. Quantitative assessment of rectal cancer response to neoadjuvant combined chemotherapy and radiation therapy: comparison of three methods of positioning region of interest for ADC measurements at diffusion-weighted MR imaging. Radiology doi:10.1148/radiol.2016151908. Published online June 2, 2016.
2. Blazic I, Maksimovic R, Gajic M, Saranovic D. Apparent diffusion coefficient measurement covering complete tumor area better predicts rectal cancer response to neoadjuvant chemoradiotherapy. Croatian Med J 2015;56(5):460–469.

Errata

Originally published in:

Radiology 2011;260(1):282–293
DOI:10.1148/radiol.11101336

Evaluation of Peripheral Arterial Disease with Nonenhanced Quiescent-Interval Single-Shot MR Angiography

Philip A. Hodnett, Ioannis Koktzoglou, Amir H. Davarpanah, Timothy G. Scanlon, Jeremy D. Collins, John J. Sheehan, Eugene E. Dunkle, Navyash Gupta, James C. Carr, Robert R. Edelman

Erratum in:

Radiology 2017;282(2):614
DOI:10.1148/radiol.2016164042

In both the abstract and main text, the first sentence of Materials and Methods should be replaced as follows: **This two-center study was approved by the institutional review board and was compliant with the Health Insurance Portability and Accountability Act. Data were collected prospectively at center one and written informed consent was obtained; at center two, data were collected retrospectively from standard of care MR angiography.**

Originally published in:

Radiology 2016;278(3):822–830
DOI: 10.1148/radiol.2015141922

Myeloperoxidase Nuclear Imaging for Epileptogenesis

Yinian Zhang, Daniel P. Seeburg, Benjamin Pulli, Gregory R. Wojtkiewicz, Lionel Bure, Wendy Atkinson, Stefan Schob, Yoshiko Iwamoto, Muhammad Ali, Wei Zhang, Elisenda Rodriguez, Andrew Milewski, Edmund J. Keliher, Cuihua Wang, Yawen Pan, Filip K. Swirski, John W. Chen

Erratum in:

Radiology 2017;282(2):614
DOI:10.1148/radiol.2016164044

The legend for Figure 2b should read as follows: Photomicrographs (**MPO staining**; original magnification, ×3100 [left] and ×3400 [right]) show that MPO-positive cells were mainly found in the hippocampal and parahippocampal regions. *MM* = macrophages and microglia.

Originally published in:

Radiology 2016;281(1):229–238
DOI: 10.1148/radiol.2016152067

Impact of Data-driven Respiratory Gating in Clinical PET

Florian Büther, Thomas Vehren, Klaus P. Schäfers, Michael Schäfers

Erratum in:

Radiology 2017;282(2):614
DOI:10.1148/radiol.2016164041

Page 229, Abstract, first line of Materials and Methods should read as follows: This **retrospective** study was approved by the ethics committee of the **Ärztekammer Westfalen-Lippe and the** University of Münster (Az 2014–217-fN).

Page 230, Patient Data and Preparation, first sentence should read as follows: The study protocol was approved by the

ethics committee of the **Ärztekammer Westfalen-Lippe and the** University of Münster.

Page 230, Patient Data and Preparation, paragraph 2, the first sentence should read as follows: Patients who were referred for a whole-body fluorine 18 fluorodeoxyglucose (FDG) PET/computed tomographic (CT) examination were included in this **retrospective** study if at least one PET-positive lesion in the thorax or upper abdomen was suspected on the basis of prior CT or PET/CT studies.

Originally published in:

Radiology 2016;281(2):527–535

DOI:10.1148/radiol.2016152244

Blood-Brain Barrier Leakage in Patients with Early Alzheimer Disease

Harm J. van de Haar, Saartje Burgmans, Jacobus F. A. Jansen, Matthias J. P. van Osch, Mark A. van Buchem, Majon Muller, Paul A. M. Hofman, Frans R. J. Verhey, Walter H. Backes

Erratum in:

Radiology 2017;282(2):615

DOI:10.1148/radiol.2016164043

Table 2, under the column Fractional Leakage Volume, Control Subjects, the value for WM should be as follows: **0.27** ± 0.14.

Originally published in:

Radiology 2017;282(2):418–428

DOI: 10.1148/radiol.2016151908

Quantitative Assessment of Rectal Cancer Response to Neoadjuvant Combined Chemotherapy and Radiation Therapy: Comparison of Three Methods of Positioning Region of Interest for ADC Measurements at Diffusion-weighted MR Imaging

Ivana M. Blazic, Gordana B. Lilic, Milan M. Gajic, PhD

Erratum in:

Radiology 2017;282(2):615

DOI:10.1148/radiol.2016164040

Five patients in this study were previously included in a 2015 study by the authors published in the *Croatian Medical Journal*. Images from this previous study, published under a Creative Commons license, were also reproduced without proper attribution. Corrections are as follows:

Third paragraph of Materials and Methods should read as follows: …and exhibit very high ADC values due to very low cellular density. **Five patients included in this study were also included in a previous study (30), in which we evaluated the accuracy of ADC measurements in assessment of rectal cancer downstaging after therapy.**

Figure 1 caption should read as follows: Areas of rectal cancer tissue (arrows) on T2-weighted MR images (top row) correspond to high-signal-intensity areas (arrows) on DW images (bottom row) in a 53-year-old male patient before CRT. **(Far left images, top and bottom, reprinted from reference 30 under a Creative Commons License.)**

Figure 2 caption should read as follows: Pre- and post-CRT T2-weighted (left column), pre- and post-CRT DW (middle column), and pre- and post-CRT ADC (right column) image sets of rectal cancer in a 53-year-old male patient who experienced complete response to CRT (tumor regression grade 1). Numbers listed on the ADC image are for the particular ROIs shown**. (Image at top right, reprinted from reference 30 under a Creative Commons License.)**

Reference 30 should be added as follows: **Blazic I, Maksimovic R, Gajic M, Saranovic D. Apparent diffusion coefficient measurement covering complete tumor area better predicts rectal cancer response to neoadjuvant chemoradiotherapy. Croatian Med J 2015;56(5):460–469.**

These errors apply to an early online version of the article and have been corrected in the final print and online article.